Journal of Molecular Liquids 356 (2022) 119043

Contents lists available at ScienceDirect

Journal of Molecular Liquids

journal homepage: www.elsevier.com/locate/molliq

A cytostatic drug from the class of triazine derivatives: Its properties in aqueous solutions, cytotoxicity, and therapeutic activity

Olga V. Mikolaichuk [a,b], Elena A. Popova [a], Alexandra V. Protas [a], Ilnaz T. Rakipov [c], Dmitry A. Nerukh [d], Andrey V. Petrov [b], Nikolay A. Charykov [e], Sergei V. Ageev [a,b], Grigorii V. Tochilnikov [f], Iulia G. Zmitrichenko [f], Aleksandr N. Stukov [f], Konstantin N. Semenov [a,b,*], Vladimir V. Sharoyko [b,a,*]

[a] Pavlov First Saint Petersburg State Medical University, 6–8 L'va Tolstogo Street, Saint Petersburg 197022, Russia
[b] Institute of Chemistry, Saint Petersburg State University, 26 Universitetskii Prospect, Saint Petersburg 198504, Russia
[c] Department of Physical Chemistry, Kazan Federal University, Kremlevskaya Street 18, Kazan 420008, Russia
[d] Department of Mathematics, Aston University, Birmingham B4 7ET, The United Kingdom
[e] Saint Petersburg State Technological Institute (Technical University), 26 Moskovskii Prospect, Saint Petersburg 190013, Russia
[f] Petrov Research Institute of Oncology, 68 Leningradskaia Street, Pesochny, Saint Petersburg 197758, Russia

ARTICLE INFO

Article history:
Received 24 December 2021
Revised 19 March 2022
Accepted 27 March 2022
Available online 31 March 2022

Keywords:
Cytostatic Agent
Solutions
Cytotoxicity
Ehrlich ascites carcinoma
Electronic structure
Molecular Dynamics

ABSTRACT

We present a comprehensive study of a water-soluble substance from the class of triazine derivatives alkylating agents. The performed physicochemical investigations of this cytostatic drug's aqueous solutions include the measurements of density, viscosity, speed of sound, refraction index, stability, solubility, distribution between water and octan-1-ol, as well as electronic structure calculations and molecular dynamics modelling. Biologically, the substance was investigated for its cytotoxicity as well as *in vitro* (on Capan-2 and SK-MEL-1 cell lines) and *in vivo* (transplantable Ehrlich ascites carcinoma model) therapeutic activity.

1. Introduction

This work continues our research on [5-[[4,6-*bis*(aziridin-1-yl)-1,3,5-triazin-2-yl]amino]-2,2-dimethyl-1,3-dioxan-5-yl]methanol (substance (a)) from the group of alkylating agents of the class of triazine derivatives (Fig. 1) [1]. 1,3,5-Triazine derivatives such as Altretamine (1) [2], Tretamine (2) [3], and Azacitidine (3) [4] (Fig. 2) are used as selective anticancer drugs against ovarian cancer [5], acute myeloid leukaemia [6], and chronic myelomonocytic leukaemia [7]. Varying the substituents at the heterocycle (triazine) allows to change the properties of the compound [8] with potentially advantageous medical effects.

Substance (a) was synthesised, investigated, and subsequently approved for medical use in the 1980s as an antineoplastic agent for the treatment of ovarian, breast, lung, kidney, liver cancers and for the prevention of regional metastasis in oral cancer [9–12]. In [13] it was shown that substance (a) is effective against abdominal carcinomatosis in animals. A detailed study of the mechanisms of action allowed to conclude that substance (a) is a small molecule from the class of alkylating agents. It is characterised by both resorptive and contact antitumour effects and it can be used for systemic and local chemotherapy, for endolymphatic chemotherapy, and chemoembolisation [14].

Previously, our group obtained data on biocompatibility and biological activity of substance (a). The data indicate high haemocompatibility, however, low affinity for human serum albumin may lead to cytotoxicity. Binding of substance (a) to deoxyribonucleic acid investigated by calorimetric titration, spectrophotometric method, and circular dichroism spectroscopy shows that substance (a) exhibits a mixed mechanism of action. Its interaction with DNA leads to the formation of covalent bonds, as evidenced by the high value of the binding constant (K_b = 3.44 10^7 M^{-1}). Experiments to study the kinetics of substance (a) interaction with DPPH, trapping of NO radicals, and photobleaching of Radachlorin show that it exhibits pronounced antioxidant activity. Cytotoxicity studies in cell lines (non-small cell lung cancer A-549, glioblastoma T98G, ovarian teratocarcinoma PA-1, pancreatic cancer PANC-1, and liver adenocarcinoma SK-HEP-1) showed a dose-dependent

* Corresponding authors at: 6–8 L'va Tolstogo Str., Saint Petersburg 197022, Russia (K.N. Semenov) and 26 Universitetskii prospect, Saint Petersburg 198504, Russia (V.V. Sharoyko).
E-mail addresses: knsemenov@gmail.com (K.N. Semenov), sharoyko@gmail.com (V.V. Sharoyko).

https://doi.org/10.1016/j.molliq.2022.119043
0167-7322/

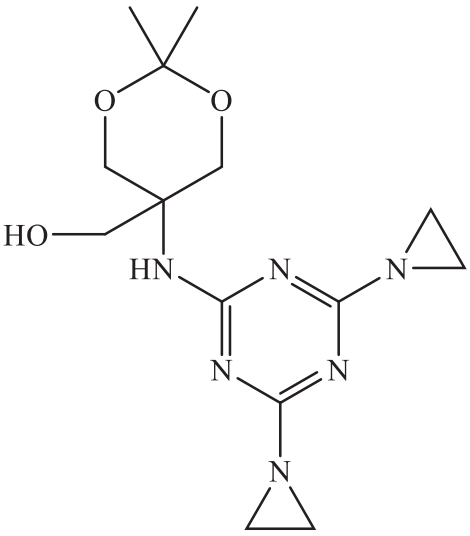

Fig. 1. The structure of substance (a).

decrease in cell survival. The greatest effect was revealed in the case of the A-549 cell line. Thus, we concluded that the cytotoxic effect of substance (a) may be due to the change of antioxidant-prooxidant balance in tumour cells and damage to DNA molecules.

This work is dedicated to a comprehensive physicochemical study of substance (a) aqueous solutions, namely, density, speed of sound, viscosity, refractive index, solubility, stability, as well as the study of structural and dynamic characteristics in the binary system substance (a) –H_2O. The physicochemical properties of a drug's aqueous solutions are extremely important in revealing the mechanism of its action [15–24]. For example, data on densities, speed of sound, viscosities allow to make conclusions about intermolecular interactions in solution, which, in turn, can determine the mechanism of the drug's biological action. The viscosity of drug containing systems is important for understanding the haemocompatibility of the test substance. The distribution coefficient allows to predict the permeability through tissue and cellular barriers, as well as the biodistribution of the drug. Stability studies are essential for understanding the pharmacokinetics, pharmacodynamics, toxicokinetics, and metabolic stability of a drug. Formulating dosage forms requires the knowledge of the active substance's compatibility with water and aqueous solutions.

2. Experimental part

2.1. Reagents

The reagents used for conducting the experiments are listed in Table S1 of Supplementary Material.

2.2. Identification methods

^1H and ^{13}C {^1H} NMR spectra were recorded on a Bruker Avance III 400 instrument (400.13 MHz for ^1H and 100.61 MHz for ^{13}C) in D_2O or in DCl, at 25 °C. High resolution mass spectral analysis was performed using Shimadzu 9030 and Bruker Daltonik GmbH 'MaXis' instruments. ^1H and ^{13}C {^1H} NMR spectra for substance (a) are in good agreement with previously published data in Ref. [1].

[5-[[4,6-*bis*(aziridin-1-yl)-1,3,5-triazin-2-yl]amino]-2,2-dimethyl-1,3-dioxan-5-yl]methanol. ^1H NMR (400 MHz, D_2O, **after 1 h**, **pH = 7**), δ: 4.15 (d, *J* = 12.3 Hz, 2H, C$\underline{H}_2$), 3.94 (d, *J* = 12.3 Hz, 2H, C$\underline{H}_2$), 3.88 (s, 2H, 2C$\underline{H}$), 2.33 (s, 8H, 4C$\underline{H}_2$), 1.42 (d, *J* = 6.1 Hz, 6H, 2C$\underline{H}_3$). HRMS (ESI$^+$), *m*/*z*: 323.1826 [M + H]$^+$, [$C_{14}H_{23}N_6O_3$]$^+$. Calculated [M + H]$^+$: 323.1828 (see Fig. S1 of the Supplementary Material).

^1H NMR (400 MHz, D_2O, **after 24 h**, **pH = 7**), δ: 4.17 (d, *J* = 12.3 Hz, 2H, C$\underline{H}_2$), 3.97 (d, *J* = 12.3 Hz, 2H, C$\underline{H}_2$), 3.90 (s, 2H, 2C$\underline{H}$), 2.36 (s, 8H, 4C$\underline{H}_2$), 1.44 (d, *J* = 6.1 Hz, 6H, 2C$\underline{H}_3$). HRMS (ESI$^+$), *m*/*z*: 323.1826 [M + H]$^+$, [$C_{14}H_{23}N_6O_3$]$^+$. Calculated [M + H]$^+$: 323.1828 (see Fig. S2 of the Supplementary Material).

NMR data of substance (a) in acidic and alkaline media was obtained as follows:

[5-[[4,6-*bis*(aziridin-1-yl)-1,3,5-triazin-2-yl]amino]-2-(hydroxymethyl)propane-1,3-diol. ^1H NMR (400 MHz, DCl, **after 1 h, pH = 3**), δ: 3.86–3.78 (m, 6H, 3C$\underline{H}_2$), 3.69 (q, *J* = 5.8 Hz, 4H, 2C$\underline{H}_2$), 2.16 (s, 8H, 4C$\underline{H}_2$). HRMS (ESI$^+$), *m*/*z*: 283.1512 [M + H]$^+$, [$C_{11}H_{19}N_6O_3$]$^+$. Calculated [M + H]$^+$: 283.1513 (see Fig. S3 of the Supplementary Material).

[5-[[4,6-*bis*(aziridin-1-yl)-1,3,5-triazin-2-yl]amino]-2-(hydroxymethyl)propane-1,3-diol. ^1H NMR (400 MHz, D_2O, **after 1 h, pH = 4**), δ: 3.70–3.62 (m, 6H, 3C$\underline{H}_2$), 3.54 (s, 4H, 2C$\underline{H}_2$), 2.07 (s, 8H, 4C$\underline{H}_2$).

[5-[[4,6-*bis*(aziridin-1-yl)-1,3,5-triazin-2-yl]amino]-2,2-dimethyl-1,3-dioxan-5-yl]methanol. ^1H NMR (400 MHz, D_2O, **after 1 h, pH = 10**), δ: 4.15 (d, *J* = 12.3 Hz, 2H, C$\underline{H}_2$), 3.94 (d, *J* = 12.3 Hz, 2H, C$\underline{H}_2$), 3.88 (s, 2H, 2C$\underline{H}$), 2.33 (s, 8H, 4C$\underline{H}_2$), 1.42 (d, *J* = 6.1 Hz, 6H, 2C$\underline{H}_3$).

Single crystals of substance (a) were selected using an optical microscope, encased in an oil-based cryoprotectant and mounted on cryoloops (Fig. 3). The measurement was carried out using a Rigaku Oxford Diffraction XtaLAB SuperNova diffractometer with an HyPix3000 CCD area detector operated with monochromated microfocused CuKα radiation (λ[CuKα] = 1.54184 Å). Experimental data processing was carried out using CrysAlisPro software. The structures were solved by direct methods and refined using the SHELX [25,26] program incorporated in the OLEX2 [27] software package.

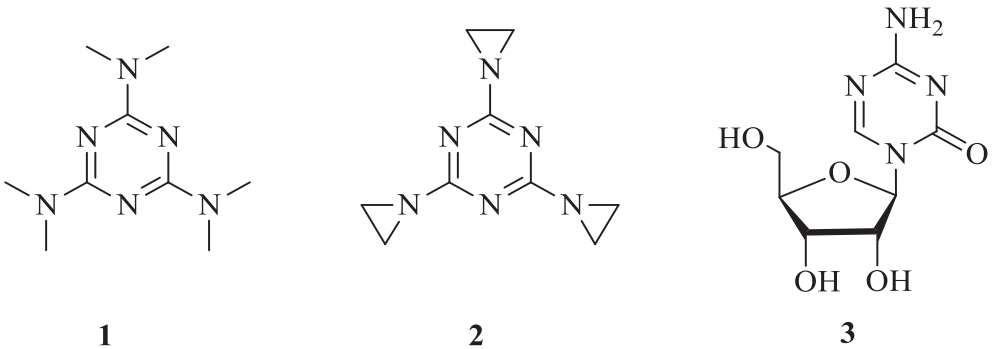

Fig. 2. The structures of anticancer drugs: Altretamine (1), Tretamine (2) and Azacitidine (3).

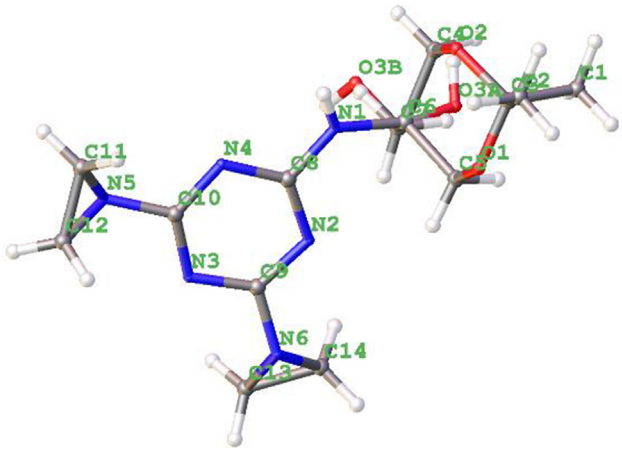

Fig. 3. Crystallographic data for substance (a) (CCDC 2074787).

2.3. Study of physicochemical properties of substance (a) aqueous solutions

The temperature and concentration dependencies of physicochemical properties in the binary system substance(a)–water were studied using following apparatus: (*i*) Anton Paar DSA 5000 (Austria) for measuring density and speed of sound; (*ii*) Lovis 2000 M Anton Paar microviscometer (Austria) for measuring viscosity; (*iii*) Automatic Multi Wavelengths Refractometer Abbemat WR/MW (Austria) for measuring refraction index. The description of experimental techniques, as well as metrological characteristics are presented elsewhere [28–40].

2.3.1. Solubility of substance (a) in aqueous solutions

The measurements of the solubility of substance (a) in water at atmospheric pressure were carried out in the temperature range T = 293.15–318.15 K with isothermal saturation method for 12 h using a thermostatically controlled shaker LAUDA ET 20 with shaking frequency of 80 Hz. The temperature was measured with an error of 0.1 K. The required volume (about 5 cm^3) was taken from the heterogeneous system at atmospheric pressure for spectrophotometric analysis. Then the liquid phase was separated by vacuum filtration for spectrophotometric analysis.

The concentration of substance (a) in a saturated solution was determined spectrophotometrically using an SF-2000 spectrophotometer (Russia). Fig. 4 presents the electronic spectrum of substance (a) at λ = 200–400 nm. Fig. 5 demonstrates the agreement with Beer–Lambert–Bouguer law (R^2 = 0.989) at λ = 220 nm. For substance (a) concentration determination in a saturated solution, the following equation was applied (at optical wavelength equal to 1 cm):

$$C = 0.049 \cdot A\ (220\ \text{nm}), \quad (1)$$

where C is the volume concentration of substance (a) (g dm^{-3}), A (220 nm) is the absorbance at λ = 220 nm.

The composition of the equilibrium crystalline hydrate of substance (a) was determined by the thermogravimetric method using NETZSCH TG 209 F1 Libra thermogravimetric analyser (Germany) in the temperature range of 40–600 °C in nitrogen atmosphere and heating rate of 5 °C·min^{-1}. Fig. 6 presents the thermogram of the crystalline hydrate of substance (a).

2.3.2. Stability of substance (a) aqueous solutions

The hydrolysis reaction of substance (a) in D_2O was studied at 25 °C by recording the ^{1}H NMR spectra of the reaction mixture

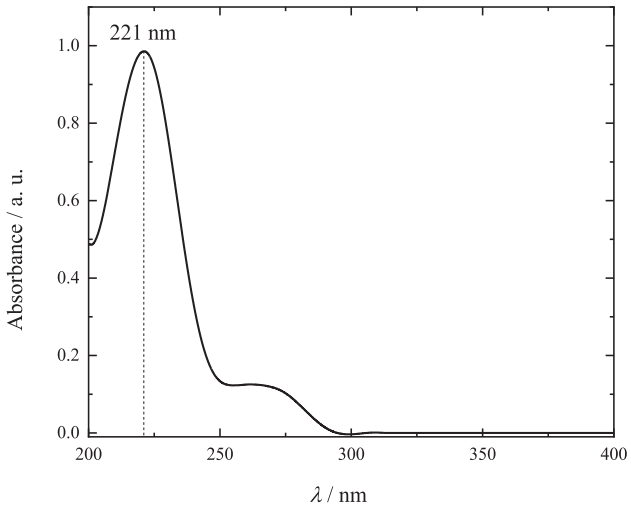

Fig. 4. The UV/Vis spectrum of substance (a) (C = 0.055 g dm^{-3}) (l = 1 cm).

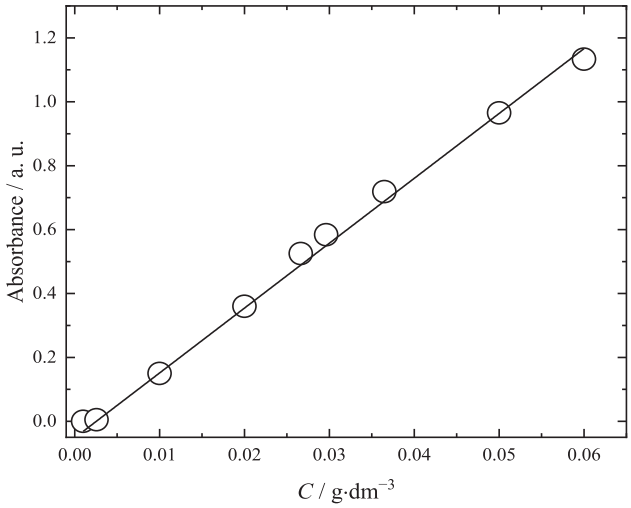

Fig. 5. Beer–Lambert–Bouguer law for substance (a) aqueous solutions (R^2 = 0.989) (λ = 221 nm).

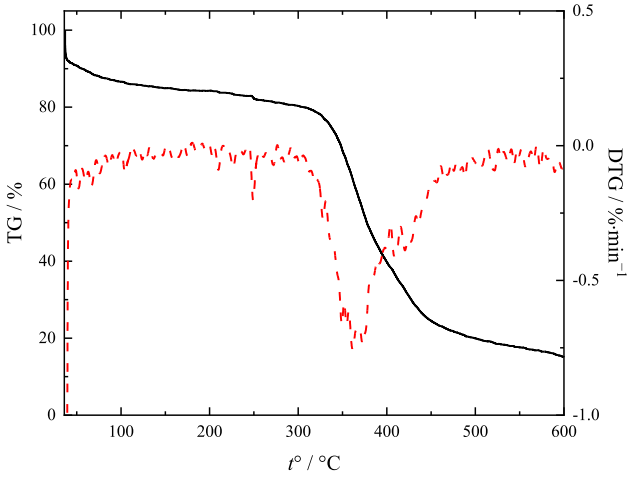

Fig. 6. TG (dashed line) and DTG (solid line) of substance (a) at t° = 40–600 °C.

on Bruker Avance III 400 (400.13 MHz) for 24 h in automatic mode with one spectrum recording every 30 min.

To study the stability of substance (a) in an acidic medium (pH = 3, 4), 20 mg of substance (a) was dissolved in 40 ml of aqueous solutions of hydrochloric acid. The resulting solution was stirred at room temperature for 45 min. At the end of the reaction, the solvent was removed under standard conditions. The product was air dried.

To study the stability of substance (a) in an alkaline medium (pH = 10), 20 mg of substance (a) was dissolved in 40 ml of an aqueous solution of 0.1 M NaOH. The resulting solution was stirred at room temperature for 1 h. At the end of the reaction, the solvent was removed under standard conditions. The product was air dried.

2.3.3. Distribution coefficient

The study of the distribution of substance (a) in the octan-1-ol–H_2O system was carried out in a shaker-thermostat LAUDA ET 20 (shaking frequency of 80 Hz). The temperature was maintained within the accuracy of 0.1 K (95% confidence interval), the time of the experiment was 5 h. For the experiment, the solution of substance (a) was prepared (C = 1 g dm^{-3}) in deionised water (electrical conductivity 5.5 10^{-6} S m^{-1}) to which an equal volume of octan-1-ol was added (25.0 ml). After reaching the equilibrium, an aliquot of the lower aqueous phase was taken. While dipping the pipette into the two-phase system, air was carefully blown through it to prevent the upper organic phase from entering the pipette. The concentration of substance (a) in the aqueous phase was measured by the spectrophotometric method using SF-2000 spectrophotometer at the wavelength λ = 220 nm according to Eq. (1). In total, five parallel measurements were carried out.

2.3.4. Membrane mitochondrial potential measurement

PANC-1 cells were trypsinised and washed with PBS (phosphate-buffered saline), containing 10% fetal bovine serum (FBS). Afterwards, the cells were resuspended in a mixture of PBS, 5% FBS and 50 mM KCl. After the incubation of the cells with MitoTracker® Orange CMTMRos fluorescent dye (500 nM) at 37 °C for 30 min, they were rinsed with PBS and plated into a black 96-well plate (80,000 cells per well). The concentration of substance (a) and doxorubicin in final suspensions were equal to 100 μM. For the dissipation of the proton gradient, 10 μM of FCCP (carbonyl cyanide-*p*-trifluoromethoxyphenylhydrazone) was added. The measurements of fluorescence was carried out using microplate reader (TECAN Instrument, Austria) at the excitation/emission wavelength of 554/576 nm.

2.3.5. Computer simulation

The study of substance (a) at the atomic/molecular level was started with the calculations of the electronic structure of the molecule. DFT calculations using DMol^3 tool from Materials Studio software package produced charges according to the Mulliken scheme. The calculations were carried out with the PBE, PW91, HCTH functionals and the DNP atomic basis (4.4). To account for the environment (vacuum, *n*-hexane, acetonitrile, water), the COSMO model was used.

The obtained charges were used to construct the electrostatic component of the force field for classical Molecular Dynamics calculations. The short-range interactions were represented by the Universal Force Field. Simulated systems consisted of one substance (a) molecule and three thousand solvent molecules in the NVT ensemble. The calculation parameters were: 5 ns simulation time, 298 K temperature, 1 fs integration step, Nosé–Hoover thermostat.

2.4. In vitro investigation of substance (a)

Substance (a) cytotoxicity towards pancreas adenocarcinoma (Capan-2) and skin melanoma (SK-MEL-1) cell lines was carried out using MTT-assay. The experimental technique is described elsewhere [1,41].

2.5. In vivo investigation of substance (a) in a transplantable Ehrlich ascites carcinoma murine model

The study was carried out in 20 female BALB/c mice which were kept under environmentally relevant conditions with a 12:12 light–dark cycle. Standard murine food and water were provided *ad libitum*. The research was approved by the Local Ethics Committee of Pavlov First Saint Petersburg State Medical University, and carried out in accordance with the University guidelines and ethical standards as well as ARRIVE guidelines. After intraperitoneal transplantation of Ehrlich ascites carcinoma, all animals were randomised into 2 groups, 10 mice per group: control mice (n = 10) and mice with administrated substance (a) at the concentration of 5 mg kg^{-1} i. p. (n = 10). Substance (a) was administered once intraperitoneally, 48 h after the tumour transplantation. The volume of the injected substance (a) 0.9% sodium chloride solution was 80 ml per kg. The control mice were injected i. p. with 0.9% sodium chloride solution of the same volume.

3. Results and discussion

3.1. Identification

Mass spectrometry and NMR spectroscopy data confirmed the composition and structure of substance (a). The signals of the protons of the aziridine groups were found in the range 2.33–2.36 ppm, and the signals at 1.42–1.44 ppm confirmed the presence of two CH_3-groups in the dioxane fragment.

Crystal Data for substance (a) $C_{14}H_{22}N_6O_3$ (M = 322.37 g mol^{-1}) were the following: triclinic, space group P-1 (no. 2), a = 9.0771(2) Å, b = 9.0823(2) Å, c = 9.8721(2) Å, α = 79.883(2)°, β = 83.960(2)°, γ = 72.365(2)°, V = 762.38(3) Å^3, Z = 2, T = 100(2) K, μ(CuKα) = 0.846 mm^{-1}, D_{calc} = 1.404 g/cm^3, 20,099 reflections measured (9.114° ≤ 2Θ ≤ 152.508°), 3089 unique (R_{int} = 0.0406, R_{sigma} = 0.0231) which were used in all calculations. The final R_1 was 0.0373 (I > 2σ(I)) and wR_2 was 0.0989 (all data). Additional X-ray diffraction data for substance (a) are presented in Tables S2–S5 of the Supplementary Material.

3.2. Study of physicochemical properties of substance (a) aqueous solutions

3.2.1. Density of aqueous solutions of substance (a)

The results of substance (a) aqueous solution density (C = 0.025–10 g·dm^{-3}, T = 293.15–333.15 K) are shown in Table S6 and Fig. 7. The average molar volumes and partial molar volumes of the solution components were obtained according to Eqs. (2) and (3):

$$\bar{V} = \frac{V}{n_{H_2O} + n_a}, \tag{2}$$

$$V_{H_2O} = \bar{V} - x_a\left(\frac{\partial \bar{V}}{\partial x_a}\right)_{T,P} \quad V_a = \bar{V} - x_{H_2O}\left(\frac{\partial \bar{V}}{\partial x_{H_2O}}\right)_{T,P} \tag{3}$$

where $\bar{V}$ is the average molar volume, V is the volume of substance (a) aqueous solution; n_{H_2O}, n_a and x_{H_2O}, x_a are the amounts of sub-

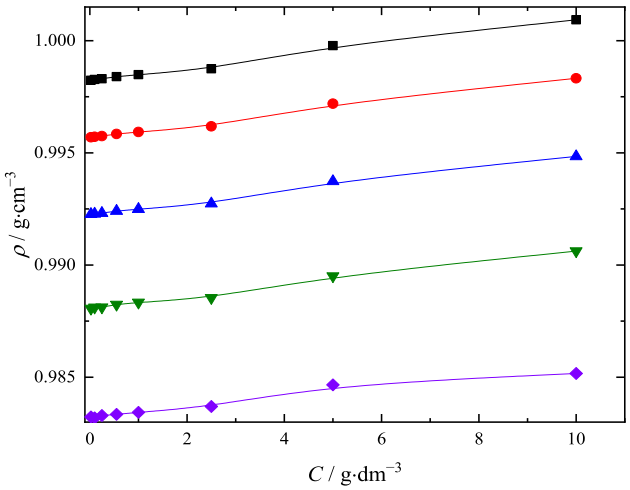

Fig. 7. Density concentration dependence of substance (a) aqueous solution at (□) 293.15 K, (○) 303.15 K, (△) 313.15 K, (▽) 323.15 K, (◇) 333.15 K.

stance and molar fractions of the solution components, respectively, V_{H_2O} and V_a are partial molar volumes of the solution components.

Figs. 8–10 present the concentration dependences of the average molar volume and the partial molar volumes in the temperature range T = 293.15–333.15 K. The results reveal that the dependence of substance (a) partial molar volume in the region of diluted solutions has a complicated shape: At low concentration up to 0.1 g dm^{-3}, the values of V_a slightly decrease. This fact shows that introducing little amount of substance (a) in the system leads to condensing and structuring of the solution.

3.2.2. Speed of sound of substance (a) aqueous solutions

Table S7 presents the values of the speed of sound in the substance (a)–H_2O system in the temperature interval T = 278.15–323.15 K. Isentropic compressibility (κ_S) was calculated according to Lalpace equation (Fig. 11):

$$\kappa_S = \rho^{-1} \cdot u^{-2}, \tag{4}$$

where ρ is the density of the solution, u is speed of sound.

Intermolecular interactions between water and substance (a) can be evaluated using the apparent specific isentropic compressibility ($\kappa_{S,\phi}$) [42–44]:

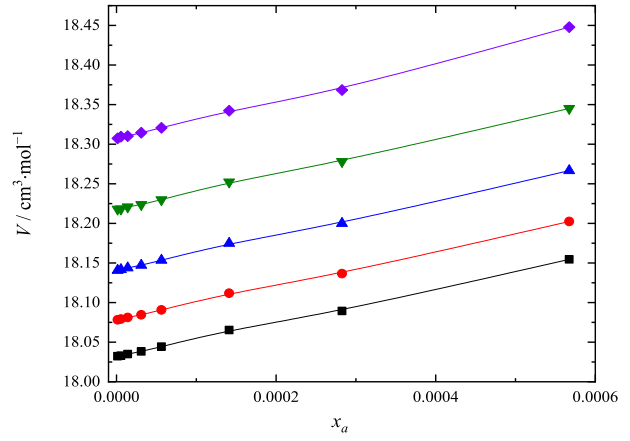

Fig. 8. Average molar volume ($\bar{V}$) concentration dependence of substance (a) aqueous solution at (□) 293.15 K, (○) 303.15 K, (△) 313.15 K, (▽) 323.15 K, (◇) 333.15 K. x_a is a molar fraction of substance (a).

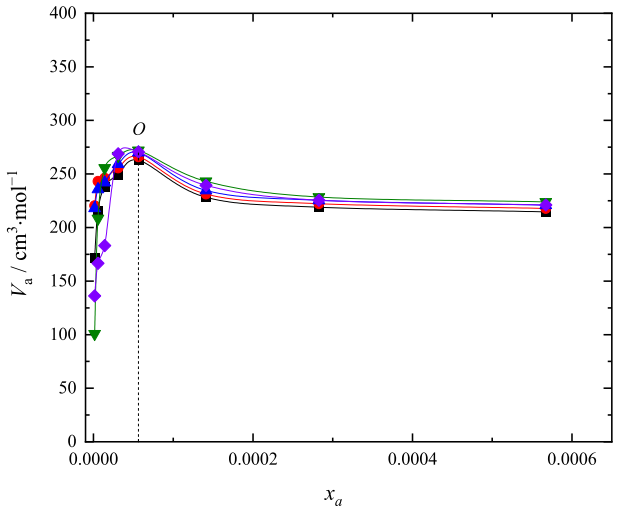

Fig. 9. $\left(\frac{\partial V}{\partial x_a}\right)_{T,P}$ derivative concentration dependence at (□) 293.15 K, (○) 303.15 K, (△) 313.15 K, (▽) 323.15 K, (◇) and 333.15 K. O is the extremum point ($\left(\frac{\partial^2 V}{\partial x^2}\right)_{T,P} = 0$, × = 5.3·10^{-6}).

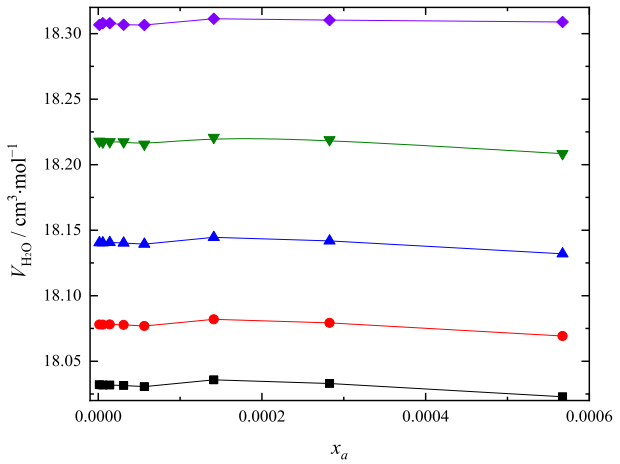

Fig. 10. Water partial volume concentration (x_a) dependence at different temperatures: (□) 293.15 K, (○) 303.15 K, (△) 313.15 K, (▽) 323.15 K, (◇) 333.15 K.

$$\kappa_{S,\phi} = \frac{\kappa_{S_a}(1 + m_a)}{\rho m_a} - \frac{\kappa_{S_{water}}}{\rho_{water} m_a}, \tag{5}$$

where m_a is the molality of substance (a), κ_{S_a} and $\kappa_{S_{water}}$ are the isentropic compressibility of solution components, ρ and ρ_{water} are the density of solution components.

Fig. 12 shows the concentration dependences of the apparent specific isentropic compressibility in the studied temperature range. The analysis of the results obtained allows to state the following: (*i*) the value of $\kappa_{S,\phi}$ is positive in the entire concentration range. This fact testifies to the high compressibility of water molecules in the binary system substance (a)–water in comparison with the one-component system. The obtained result is in good agreement with the data on the concentration dependences of the partial molar volume of substance (a) and confirms the fact of structuring and compaction of the solution in the region of low concentrations; (*ii*) a decrease in $\kappa_{S,\phi}$ with an increase in the concentration of the solute indicates that the compressibility of water molecules in the system under study approaches the compressibility of a pure solvent; (*iii*) it is obvious that an increase in temperature decreases the value of $\kappa_{S,\phi}$ due to the weakening of intermolecular interactions in the system.

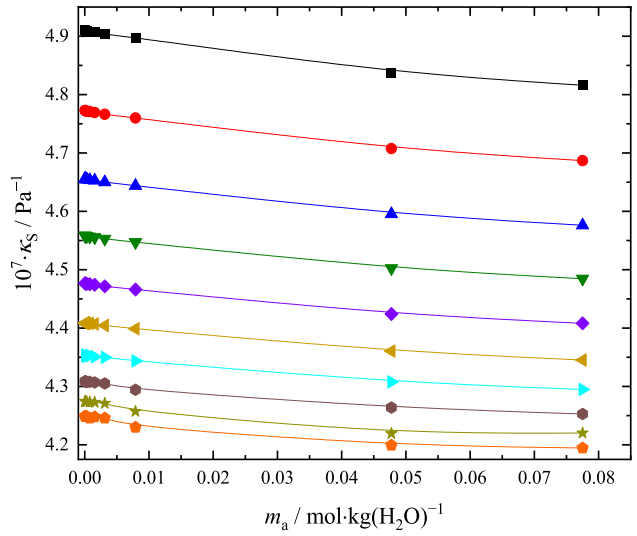

Fig. 11. Isentropic compressibility concentration dependence of substance (a) aqueous solution at (■) 278.15 K, (●) 283.15 K, (▲) 288.15 K, (▼) 293.15 K, (◆) 298.15 K, (◄) 303.15 K, (►) 308.15 K, (●) 313.15 K, (★) 318.15 K, (●) 323.15 K. *m* is molality of substance (a).

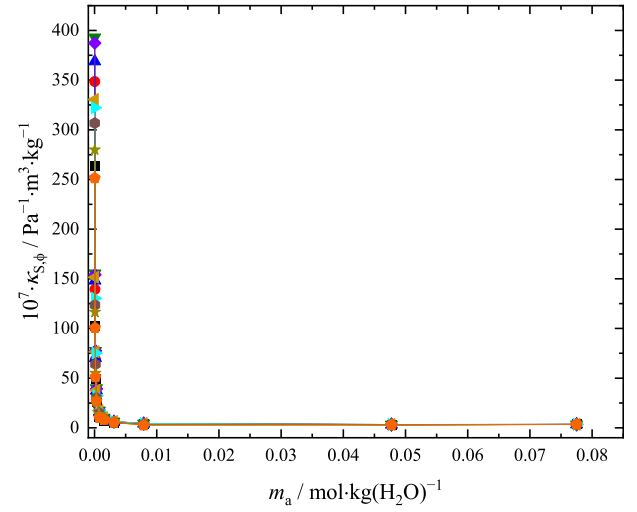

Fig. 12. Apparent specific isentropic compressibility concentration dependence of substance (a) aqueous solution at (■) 278.15 K, (●) 283.15 K, (▲) 288.15 K, (▼) 293.15 K, (◆) 298.15 K, (◄) 303.15 K, (►) 308.15 K, (●) 313.15 K, (★) 318.15 K, (●) 323.15 K.

3.2.3. Viscosity of substance (a) aqueous solutions

Table S8 presents data on the dynamic and kinematic viscosity in the binary system substance (a)–water in the temperature range T = 293.15–333.15 K. The kinematic viscosity was calculated according to Eq. (6) [45]:

$$\eta_k = \frac{\eta}{\rho}. \tag{6}$$

The thermodynamic characteristics of viscous flow activation (ΔG, ΔH, ΔS, E_a) were calculated using Eyring's theory according to the following equations (see Table 1) [45]:

$$\Delta G = RT\ln\frac{\eta V}{hN_A}, \tag{7}$$

$$\Delta G = \Delta H - T\Delta S, \tag{8}$$

$$\ln\eta = \ln A_S + \frac{E_a}{R}\frac{1}{T}, \tag{9}$$

$$T_A = \frac{-E_a}{R\ln A_S}, \tag{10}$$

where ΔG, ΔH, and ΔS are Gibbs energy, enthalpy, and entropy of viscous flow, A_S is the pre-exponential entropic factor corresponding to the viscosity at the infinite temperature, E_a is the activation energy of the transition state, T_A is the activation temperature, R is the molar gas constant, T is the absolute temperature.

The analysis of the obtained values of the thermodynamic functions of viscous flow activation allows to conclude the following: (*i*) the enthalpy values are stable and positive over the entire concentration range. This fact indicates the presence of specific interactions in solution; (*ii*) the stability of entropy values is observed over the entire concentration range. The negative definiteness of entropy indicates ordering in solution associated with the formation of an activated complex. This fact indicates the interaction between the molecules of the solute and the solvent.

The temperature dependences of the dynamic viscosity of aqueous solutions of substance (a) were described using the van't Hoff equation (Fig. 13):

$$\gamma_\eta^{\frac{\Delta T}{10}} = \frac{\eta_{T-\Delta T}}{\eta_T} = 1.21 \pm 0.05, \tag{11}$$

where γ_η is the van't Hoff viscosity coefficient.

The analysis of Fig. 13 shows that the van't Hoff temperature coefficient is constant over the studied temperature range.

Fig. 14 shows the results of applying the three-parameter Vogel–Fulcher–Tammann (VFT) equation [46] to describe the temperature dependences of the dynamic viscosity in the binary system substance (a)–water. Table 2 summarises the values of the parameters for the VFT equation, as well as the average absolute deviation (AAD) and standard deviation (SD) values.

3.2.4. Refractions of substance (a) aqueous solutions

Table S9 presents the experimental data on the refractive indices of substance (a) solutions (n_D) at C = 0.01–25 g dm^{-3} and in the temperature interval T = 293.15–333.15 K.

Specific and molar refractions of solutions were calculated using Eqs. (12) and (13):

$$r = \left(\frac{n_D^2 - 1}{n_D^2 + 2}\right) \cdot \frac{1}{\rho}, \tag{12}$$

$$R = \left(\frac{n_D^2 - 1}{n_D^2 + 2}\right) \cdot \frac{\bar{M}}{\rho}, \tag{13}$$

where r and R are the specific and molar refractions, $\bar{M}$ is the average molar mass of the solution ($\bar{M} = x_{H_2O} \cdot M_{H_2O} + x_a \cdot M_a$). We did not use the experimental data on refraction indices at low concentration region (x_a < 1.4 10^{-4}) due to low accuracy (see Table 3).

The specific (r) and molar (R) refractions of substance (a) were calculated according to Eqs. (14) and (15):

$$r = (r_{H_2O} \cdot w_{H_2O} + r_a \cdot w_a) \cdot \frac{1}{100}, \tag{14}$$

$$R = R_{H_2O} \cdot x_{H_2O} + R_a \cdot x_a, \tag{15}$$

where r_i, R_i are specific and molar refractions of the solution components, w_i, x_i are the mass and molar fractions of the solution components (see Table 3).

Additionally, the substance (a) molar refraction was estimated using the Eisenlohr (Eq. (16)) and Vogel (Eq. (17)) additivity rules [47]:

Table 1
Viscous flow activation parameters for substance (a) aqueous solutions.

C/g dm^{-3}	E_a/J·mol^{-1}	lnA_s/ln[mPa·s]	T_A/K	ΔH/kJ·mol^{-1}	ΔS/J·mol^{-1}
0.025	15118.67	−6.21	292.94	14.81	−5.09
0.10	15099.15	−6.20	292.88	14.79	−5.15
0.25	15115.69	−6.21	292.94	14.81	−5.10
0.55	15108.14	−6.20	292.94	14.80	−5.13
1.0	15052.56	−6.18	293.04	14.75	−5.33
2.5	15124.00	−6.20	293.22	14.82	−5.12
5.0	15187.55	−6.22	293.87	14.88	−5.01
10	15091.71	−6.15	295.35	14.77	−5.62

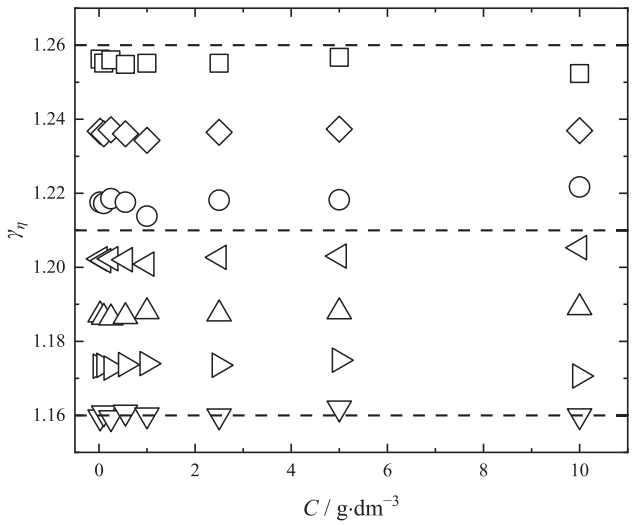

Fig. 13. Van't Hoff viscosity coefficient concentration dependence in substance (a) aqueous solutions. (□)$\frac{\eta_{278.15}}{\eta_{288.15}}$, (○)$\frac{\eta_{283.15}}{\eta_{293.15}}$, (△)$\frac{\eta_{288.15}}{\eta_{298.15}}$, (▽)$\frac{\eta_{293.15}}{\eta_{303.15}}$, (◇)$\frac{\eta_{298.15}}{\eta_{308.15}}$, (◁)$\frac{\eta_{303.15}}{\eta_{313.15}}$, (▷)$\frac{\eta_{308.15}}{\eta_{318.15}}$, (○)$\frac{\eta_{313.15}}{\eta_{323.15}}$.

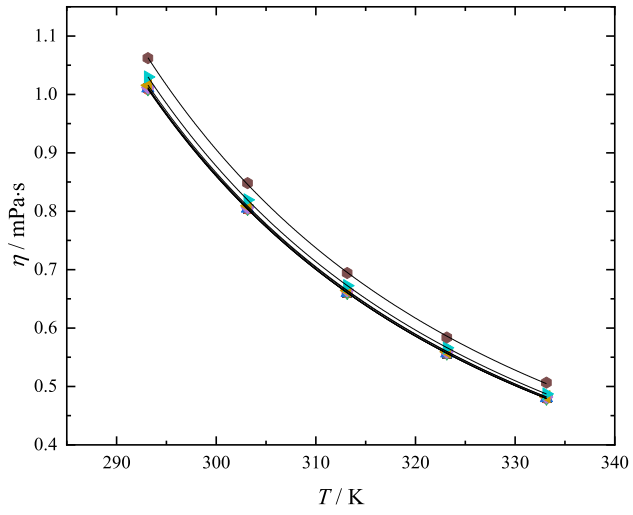

Fig. 14. Dynamic viscosity temperature dependences with a shear rate of 100 s^{-1} of substance (a) aqueous solutions at C = (□) 0.1 g dm^{-3}, (○) 0.25 g dm^{-3}, (△) 0.5 g dm^{-3}, (▽) 1 g dm^{-3}, (◇) 2.5 g dm^{-3}, (◁) 5 g dm^{-3}, (▷) 10 g dm^{-3}, (○) 15 g dm^{-3}.

$$R^{add} = 14R_C + 22R_H + R_{O(OH)} + 2R_{O(R-O-R')} + R_{N(R_2NH)} + 2R_{N(R_3N)} + 3R_{N(C-N=C)} \approx 83.345\ cm^3 \cdot mol^{-1}, \quad (16)$$

$$R^{add} = 20R_{C-H} + 11R_{C-N} + 7R_{C-C} + 5R_{C-O} + 3R_{C=N} + R_{O-H} + R_{N-H} \approx 82.262\ cm^3 \cdot mol^{-1}. \quad (17)$$

The specific refraction of substance (a) was determined using Eq. (18):

$$r^{add} = \frac{R^{add}}{M_a}. \quad (18)$$

The obtained values are equal to 0.259 cm^3 g^{-1} (calculated from the molar refractions according to Eisenlohr rule) and 0.255 cm^3 g^{-1} (calculated from the molar refractions according to Vogel rule).

The comparison between experimental and calculated data on specific (a) and molar refractions (b) are presented in Fig. 15. One can see good correspondence between the results.

3.2.5. Correlation of physicochemical properties of substance (a) aqueous solutions

T–C data on investigated physicochemical properties of substance (a) aqueous solutions (density, speed of sound, viscosity, and refraction index) were fitted using Eq. (19):

$$M = a + \sum_{i=1}^{4} b_i \cdot T^i + \sum_{j=1}^{4} c_j \cdot C^j, \quad (19)$$

where M is the property under correlation, a, b_i, c_j (i, j = 1–4) are the fitting parameters obtained using the least-square method in OriginLab software (Table 4, Fig. 16).

3.3. Substance (a) solubility

Fig. 17 presents the experimental values of the solubility of substance (a) in water (T = 293.15–318.15 K). It can be seen that substance (a) is well soluble in water. The solubility values varied in the range 26.3–43.0 g dm^{-3} in the studied temperature range. It is clearly seen that the temperature dependence of solubility has a sigmoidal form. At the same time, the solubility rises with temperature increase. This fact determines that dissolution of substance (a) in water is accompanied with an endothermic effect. Conducted thermogravimetric analysis shows that the equilibrium solid phase with saturated solution is a crystalline hydrate of substance (a) of composition $C_{14}H_{22}N_6O_3$ $3H_2O$.

3.4. Study of the stability of substance (a) in aqueous solutions by NMR spectroscopy

The effect of the solvent on the stability of substance (a) was investigated by measuring the kinetics of the reaction by ^{1}H NMR spectroscopy. During the experiment, the intensity did not decrease, and displacement of the signals corresponding to the protons of the parent compound was not recorded. Within 24 h, no changes were found in the original spectra. Fig. 18 shows the fragments of ^{1}H NMR spectra recorded at regular intervals in an

Table 2
Correlation parameters for the VFT equation ($\lg\eta(T) = \lg\eta_0 + \frac{A}{T-B}$).

Parameter	C/g dm^{-3}							
	0.025	0.1	0.25	0.55	1	2.5	5	10
$\lg\eta_0$/lg[mPa s]	−1.3096	−1.3241	−1.3032	−1.3321	−1.3267	−1.3254	−1.3295	−1.2895
A/K	160.8	165.1	159.0	167.4	166.9	165.9	168.0	161.6
B/K	170.8	168.8	171.5	167.9	167.8	168.6	168.0	170.4
SD/mPa s	0.00048	0.00032	0.00062	0.00039	0.00071	0.00064	0.00026	0.00277
AAD/%	0.17	0.12	0.12	0.12	0.12	0.03	0.07	0.23

Table 3
Refraction properties of substance (a) aqueous solutions at 293.15 K.

w/%	x 10^3	n_D	r/cm^3 g^{-1}	R/cm^3 mol^{-1}	r_a/cm^3 g^{-1}	R_a/cm^3 mol^{-1}
0.0025	0.0014	1.3330	0.2060	3.7088	–	–
0.010	0.0056	1.3330	0.2060	3.7091	–	–
0.025	0.014	1.3330	0.2061	3.7096	–	–
0.050	0.031	1.3331	0.2061	3.7106	–	–
0.10	0.056	1.3331	0.2061	3.7122	–	–
0.25	0.14	1.3332	0.2062	3.7175	0.4451	127.46
0.50	0.28	1.3338	0.2062	3.7264	0.3257	96.85
1.00	0.57	1.3345	0.2064	3.7442	0.2862	81.54
1.50	0.85	1.3353	0.2066	3.7622	0.2748	76.47
2.50	1.44	1.3369	0.2070	3.7991	0.2649	72.45

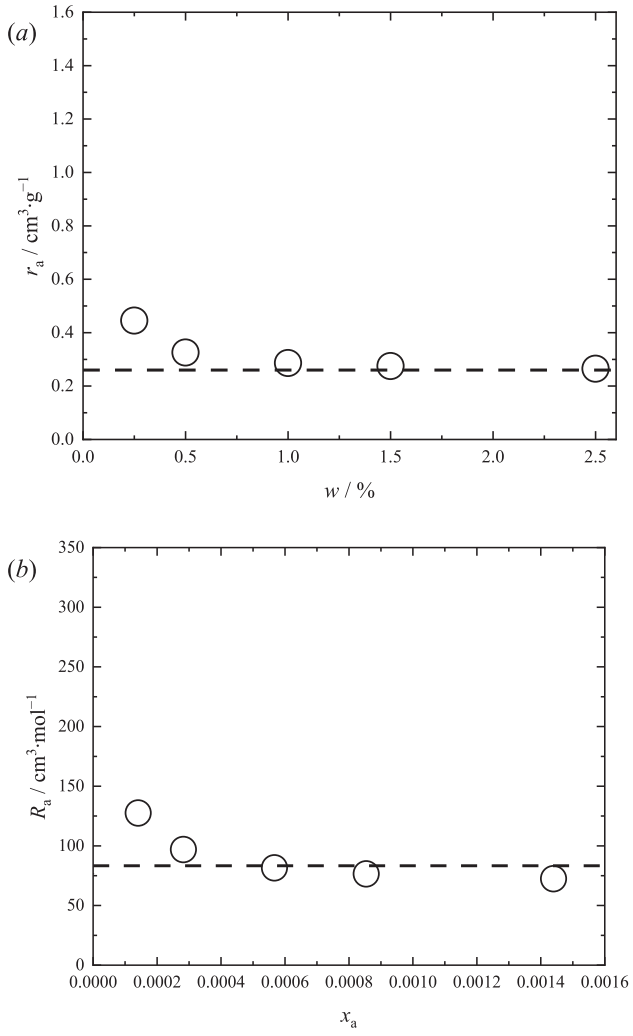

Fig. 15. Specific (*a*) and molar (*b*) refractions concentration dependence in aqueous solutions at 293.15 K. w is the mass fraction of substance (a), x_a is the molar fraction of substance (a).

automatic mode. There is no visible shift of signals or decrease in their intensity over time. Thus, it can be concluded that substance (a) is stable at pH = 7 at least for 24 h.

In addition, we investigated the influence of pH on the stability of substance (a) in solutions at pH = 3, 4, and 10. Substance (a) containing the 1,3-dioxane fragment in its structure undergoes hydrolysis under the action of acid catalysts. In this case, the electron-donating substituents in position 2 accelerate the rate of hydrolysis (Fig. 19). Thus, the 1,3-dioxane moiety can undergo hydrolysis to form *tris*(hydroxymethyl)aminomethane (b) according to Fig. 19 [48].

It was found by NMR spectroscopy that at pH 3 and 4, the disappearance of the signals is observed from the protons of the CH_3-groups (1.41–1.42 ppm), as well as the shift of the chemical shifts of the CH_2-protons of aziridine rings in a strong field (from 2.33 to 2.16 and 2.07 ppm, respectively). These changes may indicate the hydrolysis of the 1,3-dioxane fragment with the formation of the *tris*(hydroxymethyl)aminomethane derivative (b) at pH 3 and 4 (Fig. 20). The formation of product (b) was also confirmed by mass spectrometry.

It was found by NMR spectroscopy that no noticeable shift of signals occurs in an alkaline medium at pH = 10. Thus, it can be concluded that the structure of substance (a) is stable in an alkaline medium (Fig. 21).

3.5. Distribution in the octan-1-ol–H_2O system

The substance (a) distribution coefficient between phases was calculated using Eq. (20):

$$P_{ow} = \frac{c'_o}{c'_w} = \frac{c_w - c'_w}{c'_w}, \quad (20)$$

where c'_o and c'_w are the concentrations of substance (a) in octan-1-ol and water, respectively, after distribution, c_w is the initial concentration of substance (a) in water.

The obtained value for substance (a) turned out to be $\lg P_{ow}$ = 0.16 ± 0.01. The indicated value shows that substance (a) has practically the same affinity for the aqueous and lipid phases. The literature data contain only one calculated value for the octan-1-ol–water partition coefficient of substance (a): $\lg P_{ow}$ = 0.1 [49]. This value was obtained using the XLOGP3-AA method [50]. XLOGP3-

Table 4
Fitting parameters a, b_i, c_j (i, j = 1–4) for T–C dependences of density (ρ), speed of sound (u), viscosity (η), and refraction indices (n_D) of substance (a) aqueous solutions according to Eq. (19). R^2 is the coefficient of determination.

Solution property	a	b_1	b_2	b_3	b_4	c_1	c_2	c_3	c_4	R^2
ρ/g cm^{-3}	−5.12	0.076	−3.53 10^{-4}	7.32 10^{-7}	−5.76 10^{-10}	3.70 10^{-4}	−1.57 10^{-4}	4.26 10^{-5}	−2.81 10^{-6}	0.99967
u/m s^{-1}	−14072.04	161.83	−0.64	1.15 10^{-3}	−8.00 10^{-7}	0.48	0.11	−0.011	2.75 10^{-4}	0.99978
η/mPa·s	507.88	−6.04	0.027	−5.46 10^{-5}	4.13 10^{-8}	3.24 10^{-3}	−1.18 10^{-3}	3.07 10^{-4}	−1.84 10^{-5}	0.99960
n_D	2.49	−0.016	8.24 10^{-5}	−1.87 10^{-7}	1.56 10^{-10}	1.64 10^{-4}	−1.32 10^{-6}	1.04 10^{-7}	−2.03 10^{-9}	0.99926

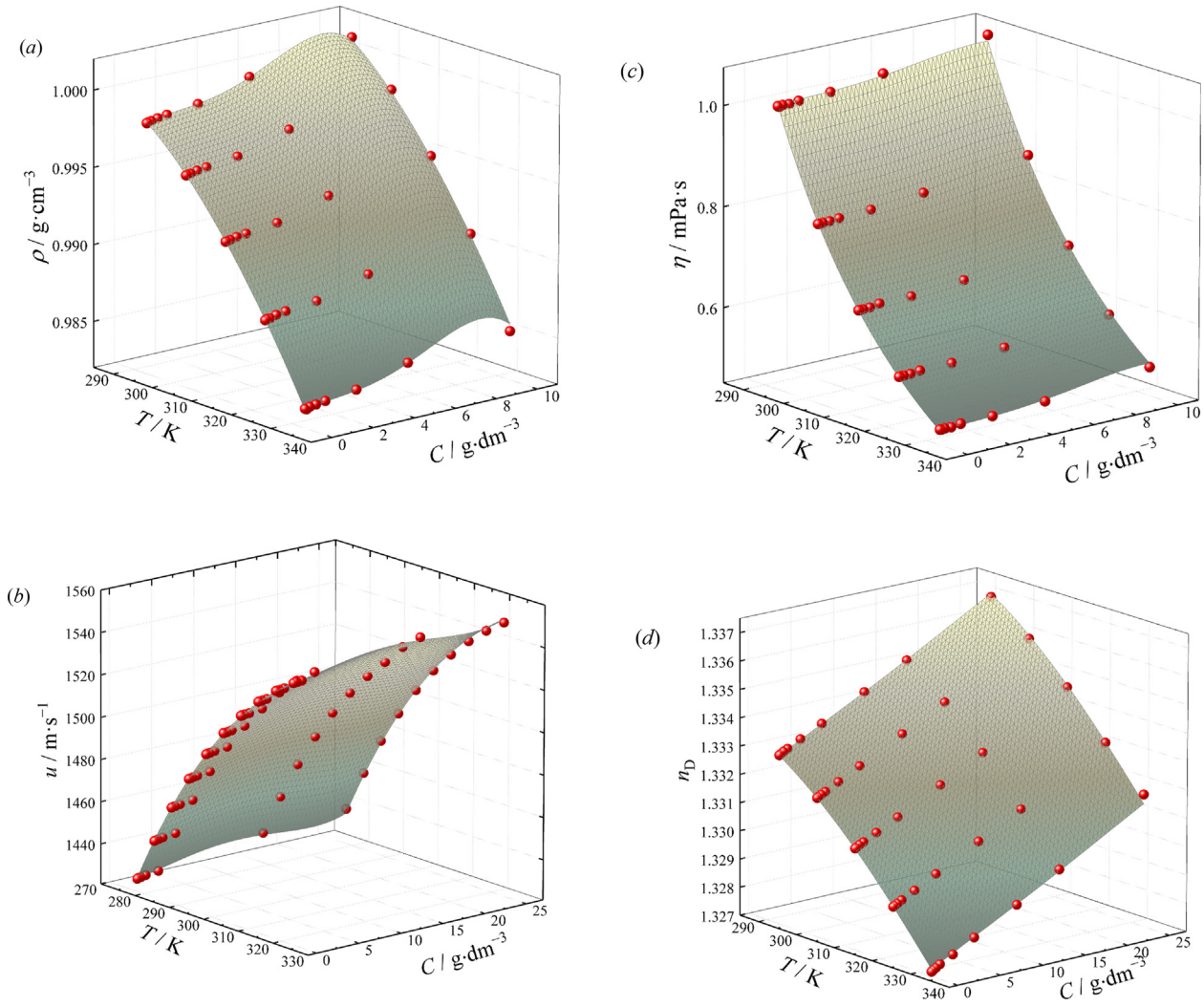

Fig. 16. T–C dependences of substance (a) aqueous solutions density (*a*), speed of sound (*b*), dynamic viscosity (*c*), refraction index (*d*). Spheres are experimental data; surfaces are calculated data.

AA is an atom-additive method that calculates lgP_{ow} by adding up contributions from each atom in the given molecule.

3.6. Membrane mitochondrial potential

As known from the literature, the mechanism of the cytotoxic action of doxorubicin is to inhibit the activity of topoisomerase II, which leads to inhibiting DNA replication and damage to mitochondria due to the inhibition of complex I of the electron donor chain and the decrease in the mitochondrial potential [51]. The combination of these factors causes mitochondrial damage and activation of oxidative stress.

The study showed that doxorubicin reduces the mitochondrial membrane potential by 45 ± 5% compared to the control. In the case of substance (a) no statistically significant effect on the value of the mitochondrial membrane potential was observed. Thus, based on the results of previous studies [1], we can conclude that the key mechanism of the cytostatic action of substance (a) is the damaging effect on the DNA molecule.

3.7. Electronic structure and molecular dynamics

The results of calculating charges (average values for each type of atoms) for various functionals and environments are given in Table 5. An increase in the dielectric constant of the medium leads to an increase in the absolute values of the charges on the atoms. In this case, the highest negative values belong to the oxygen atoms of the molecule. This means that the interaction with polar solvents, in particular, solvation and hydrolysis will mainly be carried out *via* carbon–oxygen bonds.

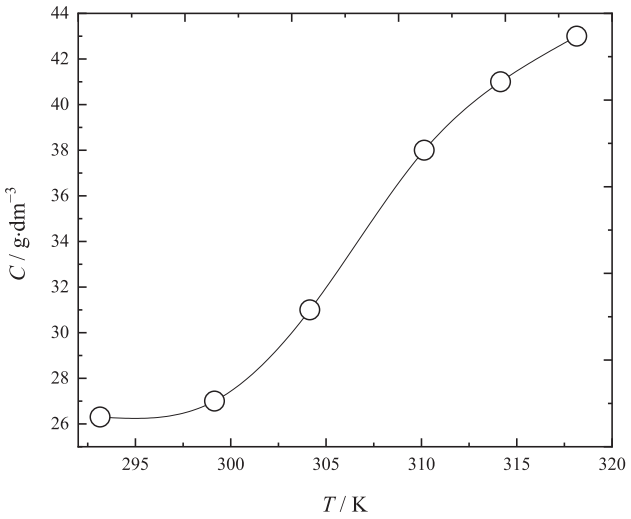

Fig. 17. Polythermal solubility of substance (a).

Molecular dynamics calculations have confirmed this approach. Table 6 shows the maxima of the radial distribution functions (RDF) between water molecules and the corresponding atoms of substance (a) (for designation, see Fig. 22). The closest approach of water molecules to oxygen atoms of substance (a) increases the higher probability of breakage of carbon–oxygen bonds due to the hydrolysis.

3.8. Cytotoxicity

The study of the cytotoxicity of substance (a) in relation to the cell lines Capan-2 (Fig. 23) and SK-MEL-1 (Fig. 24) shows dose-dependent decrease in cell survival in the concentration range C = 0.098–50 μM. Fig. 25 summarises the data on the cytotoxicity of substance (a) on various cell lines in comparison with such widely used cytotoxic drugs as doxorubicin and cisplatin. It can be seen that substance (a) has the most pronounced effect towards the A549 cell line (human adenocarcinomic cells), superior to that of doxorubicin and cisplatin. In the case of other cell lines, the effect of substance (a) is comparable to that of cisplatin and is inferior in effectiveness to doxorubicin. Separately, it should be noted that substance (a) has the lowest cytotoxicity towards healthy HEK293 cells (human embryonic kidney cells) in comparison with doxorubicin and cisplatin. The observed effect indicates a lower cytotoxicity of substance (a).

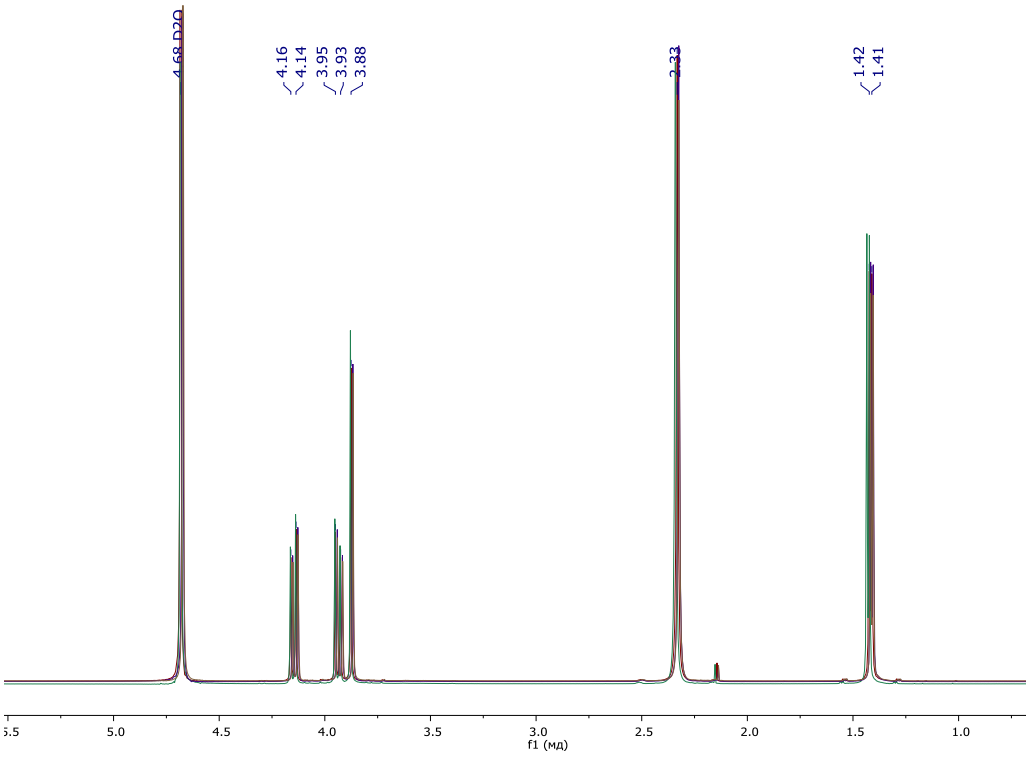

Fig. 18. ^{1}H NMR spectra of substance (a) in D_2O after 24 h (pink), 20 h (blue), 16 h (green) and 12 h (red). (For interpretation of the references to colour in this figure legend, the reader is referred to the web version of this article.)

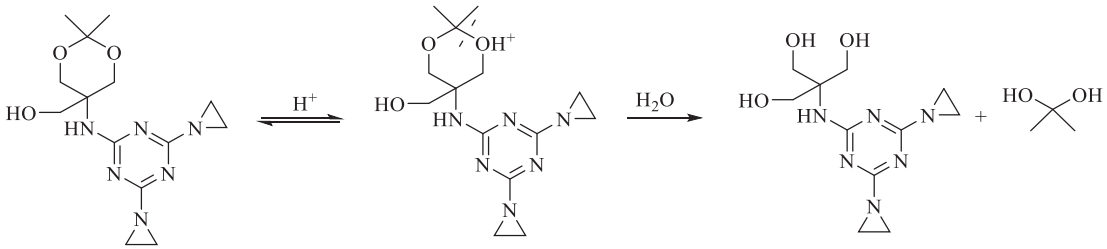

Fig. 19. Hydrolysis scheme of substance (a).

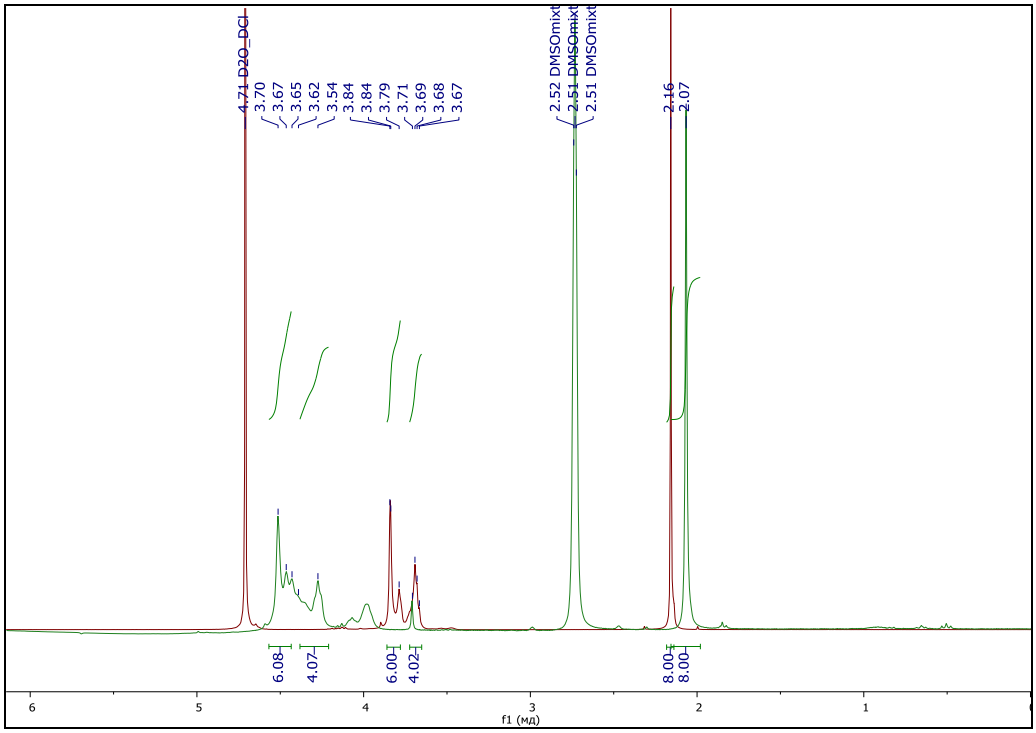

Fig. 20. [1]H NMR spectra after hydrolysis of substance (a) at pH = 3 (red) and pH = 4 (green). (For interpretation of the references to colour in this figure legend, the reader is referred to the web version of this article.)

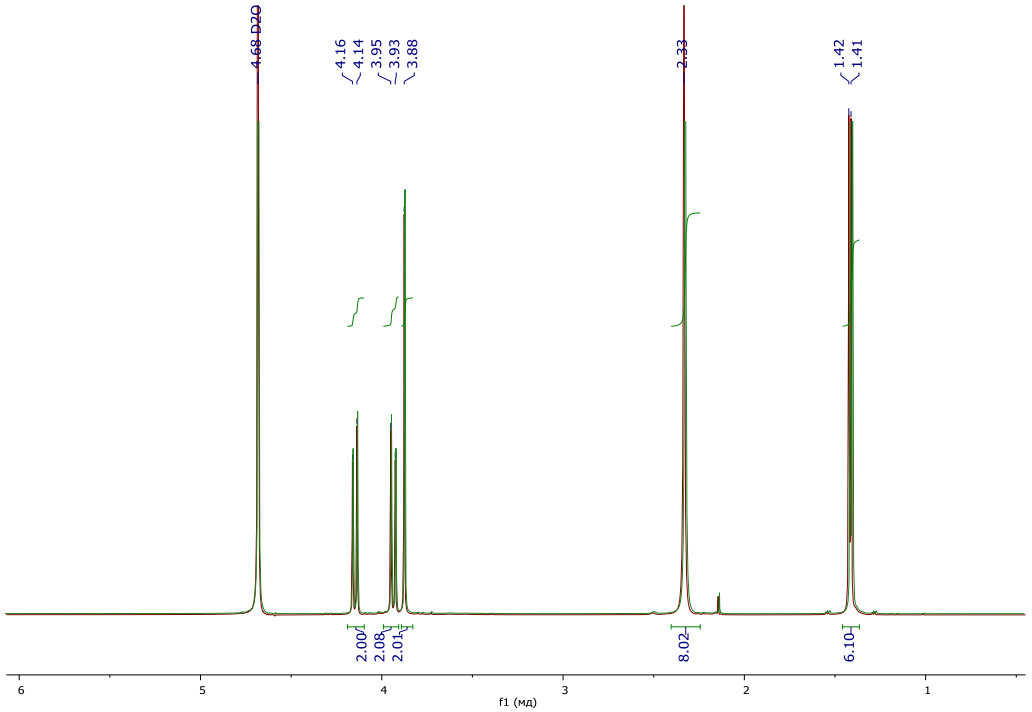

Fig. 21. [1]H NMR spectra of substance (a) in D_2O (red) and at pH = 10 (green). (For interpretation of the references to colour in this figure legend, the reader is referred to the web version of this article.)

3.9. Ehrlich ascites carcinoma murine model

By the 8th day after tumour transplantation, the ascites was observed in all control mice and was completely absent in the animals that received substance (a). Only by the 18th day the ascites was observed in all mice of the substance (a) group (Table 7).

The lag in the accumulation of ascites under the influence of substance (a) was reflected in the body weight of the animals. By

Table 5
Average charges on substance (a) atoms.

Medium	ε	Carbon	Nitrogen	Hydrogen	Oxygen
PBE					
Vacuum	1	0.276	−0.335	0.270	−0.476
n-Hexane	1.89	0.281	−0.338	0.279	−0.485
Acetonitrile	37.5	0.287	−0.342	0.294	−0.507
Water	78.54	0.288	−0.342	0.294	−0.507
PW91					
Vacuum	1	0.271	−0.334	0.270	−0.489
n-Hexane	1.89	0.276	−0.337	0.213	−0.499
Acetonitrile	37.5	0.282	−0.339	0.217	−0.519
Water	78.54	0.283	−0.341	0.294	−0.520
HCTH					
Vacuum	1	0.340	−0.373	0.257	−0.500
n-Hexane	1.89	0.345	−0.377	0.204	−0.507
Acetonitrile	37.5	0.348	−0.381	0.279	−0.527
Water	78.54	0.352	−0.381	0.270	−0.527

Table 6
The values of the maxima of the RDF between substance (a) atoms and water (for designation, see Fig. 22).

Atom type	N4	N5	N6	N7	N8	N9	O1	O2	O3
RDF/Å	3.65	3.71	3.95	3.59	4.79	3.55	3.57	3.49	3.43

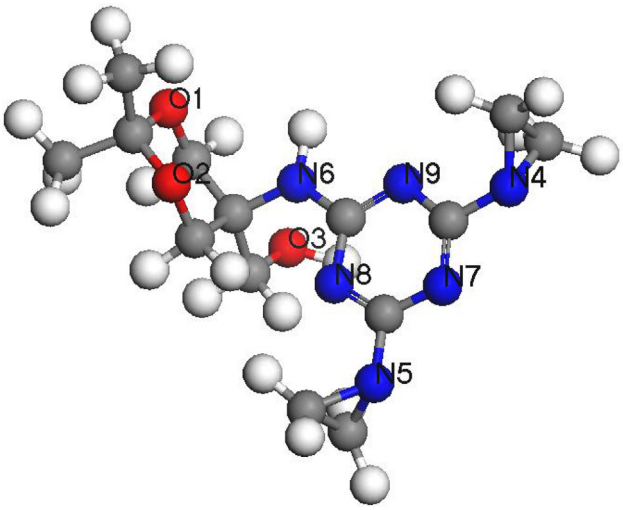

Fig. 22. Structure of substance (a) with allocated oxygen and nitrogen atoms.

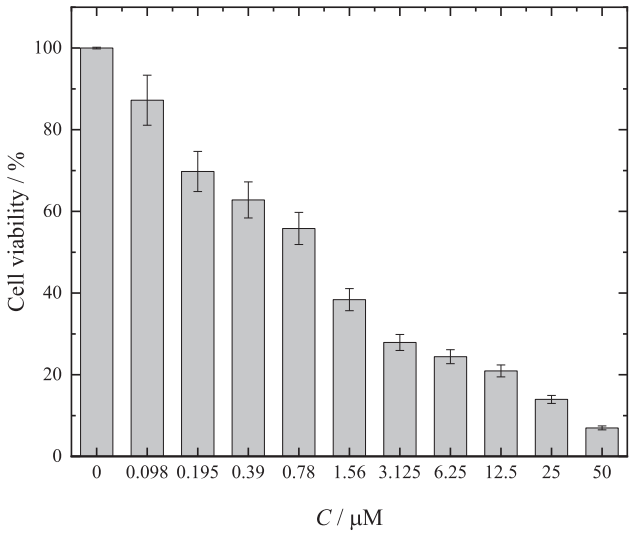

Fig. 23. Effect of substance (a) on Capan-2 cell line viability.

the 12th day after the tumour transplantation, while the body weight of the control mice increased by 14% (p = 0.0259), the body weight of the mice that received substance (a) did not differ from the initial weight, and only by the 16th day an increase in the body weight was recorded (Table 8). The delay in tumour development under the influence of substance (a) resulted in increased life expectancy of the animals (Fig. 26).

By the 24th day after transplantation, when 100% of the control mice died, 80 % of the animals in the group of mice injected with substance (a) remained alive (p = 0.0003). As a result of substance (a) treatment, the risk of death from the tumour decreased by 69% (HR 0.3099; 95% CI 0.1105–0.8691; p = 0.0006). The life expectancy median for the mice that received substance (a) increased by 42% in comparison with the control group (Table 9).

The obtained results suggest the presence of a contact antitumor effect of substance (a). This property allows to consider its use as promising treatment in other approaches of local chemotherapy, including hyperthermic chemoperfusion of the abdominal cavity and intra-arterial perfusion. The contact cytotoxicity of substance (a) can also be clinically used in intravesical chemotherapy for superficial bladder cancer. Due to its amphiphilicity, substance (a) can be used in oil solutions for chemoembolisation in patients with primary and metastatic liver cancer and in kidney cancer.

4. Conclusions

We present novel experimental data on the physicochemical properties of substance (a) aqueous solutions. It was revealed that the presence of substance (a) in aqueous solution leads to solution structuring. It was shown that substance (a) is compatible with water and demonstrates high stability in time in neutral and alkaline medium. The investigated distribution of substance (a) between octan-1-ol and water has shown that its affinity is compa-

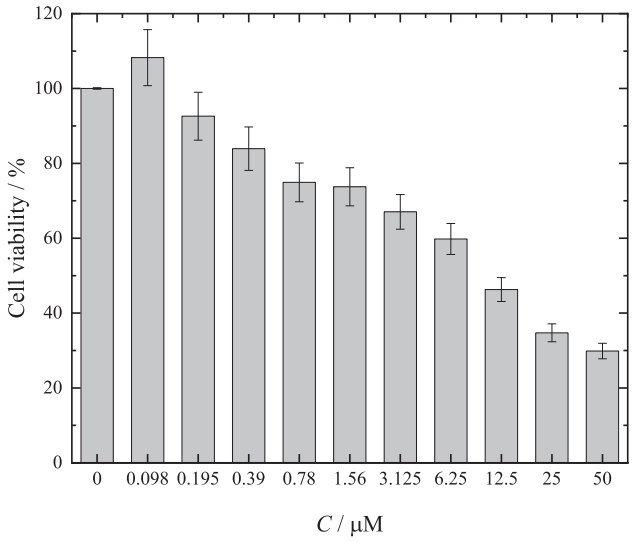

Fig. 24. Effect of substance (a) on SK-MEL-1 cell line viability.

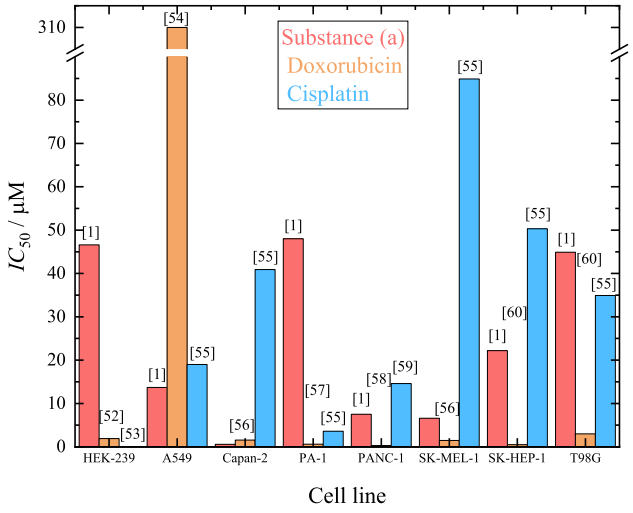

Fig. 25. Comparison of IC_{50} values of substance (a) (left column), doxorubicin (middle column), and cisplatin (right column) for the following cell lines: HEK293, A549, Capan-2, PA-1, PANC-1, SH-MEL-1, SK-HEP-1, and T98G. Columns with numbers indicate literature data references [1,52–60].

Table 7
Effect of substance (a) on the timing of ascites in BALB/c mice with Ehrlich carcinoma.

Days after transplantation	Number (%) of mice without ascites		*p*
	Control	Substance (a)	
8	0 (0%)	10 (100%)	$<10^{-4}$
10	0 (0%)	10 (100%)	$<10^{-4}$
12	0 (0%)	10 (100%)	$<10^{-4}$
14	0 (0%)	9 (90%)	10^{-4}
16	0 (0%)	5 (50%)	$9.8\ 10^{-3}$
18	0 (0%)	0 (0%)	

rable for the aqueous and lipid phases. A dose-dependent cytostatic effect of substance (a) was shown on Capan-2 and SK-MEL-1 cell lines. The measurement of the mitochondrial membrane potential did not reveal the effect of substance (a) on the functional activity of mitochondria. The therapeutic activity of intraperitoneal

Table 8
Effect of substance (a) on body weight change in BALB/c mice with Ehrlich ascites tumour.

Days after transplantation	Control (n = 10)		Substance (a) 5 mg kg^{-1} (n = 10)	
	Body mass	% to the original	Body mass	% to the original
0	35.6 ± 0.8	100%	35.3 ± 0.7	100%
6	36.3 ± 1.1	102% p = 0.5241	33.9 ± 0.8	96% p = 0.1864
8	39.2 ± 1.0	110% p = 0.0112	33.9 ± 1.0	96% p = 0.2302
10	39.4 ± 1.0	111% p = 0.0085	34.6 ± 0.9	98% p = 0.4915
12	40.6 ± 1.2	114% p = 0.0033	35.4 ± 0.7	100% p = 0.6827
14	39.7 ± 1.5	112% p = 0.0259	35.5 ± 1.1	100% p = 0.8804
16	40.2 ± 2.2	113% p = 0.0541	38.3 ± 1.3	113% p = 0.0121

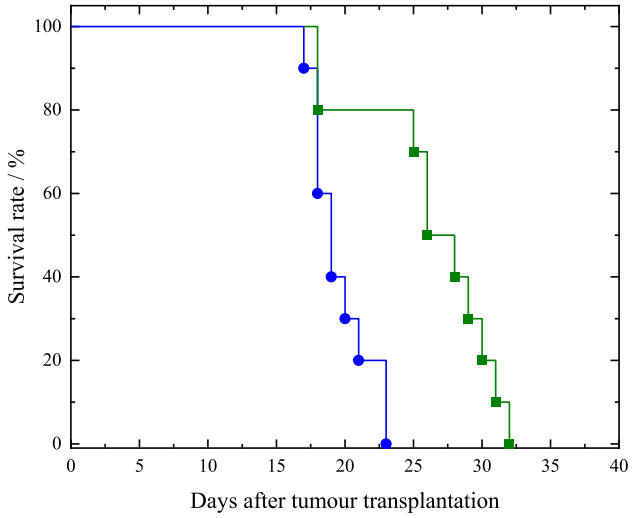

Fig. 26. Effect of substance (a) on the survival of mice with Ehrlich ascites carcinoma, where ○ marks the control group and □ marks the substance (a) group.

Table 9
Effect of substance (a) on the life expectancy median of mice with Ehrlich ascites carcinoma.

Group	Number of mice/ alive over 60 days (%, *p*)	Life expectancy median (days)	75% confidence interval	Increase in life expectancy	*p* (Mann–Whitney test)
Control	10/0	19.00	18.00–21.50	–	–
Substance (a)	10/0	27.00	23.75–30.25	42%	0.0060

administration of substance (a) in chemotherapy of abdominal carcinomatosis was established in the model of Ehrlich ascites carcinoma. All results combined are of interest for further medical applications of substance (a).

CRediT authorship contribution statement

Olga V. Mikolaichuk: Investigation, Resources. **Elena A. Popova:** Investigation, Resources, Data curation. **Alexandra V. Pro-**

tas: Investigation, Resources. **Ilnaz T. Rakipov:** Investigation. **Dmitry A. Nerukh:** Investigation, Visualization. **Andrey V. Petrov:** Investigation, Visualization. **Nikolay A. Charykov:** Investigation, Data curation. **Sergei V. Ageev:** Writing – review & editing, Data curation, Visualization. **Grigorii V. Tochilnikov:** Investigation, Resources, Data curation. **Iulia G. Zmitrichenko:** Investigation, Resources. **Aleksandr N. Stukov:** Investigation, Resources. **Konstantin N. Semenov:** Project administration, Funding acquisition. **Vladimir V. Sharoyko:** Conceptualization, Validation, Supervision, Project administration.

Declaration of Competing Interest

The authors declare that they have no known competing financial interests or personal relationships that could have appeared to influence the work reported in this paper.

Acknowledgements

The work was supported by Russian Foundation for Basic Research (project number 21-515-10007). The equipment of the following Resource Centres of the Research Park of Saint Petersburg State University was used: Resource Centre 'GeoModel', the Centre for Diagnostics of Functional Materials for Medicine, Pharmacology and Nanoelectronics, Interdisciplinary Resource Centre for Nanotechnology, Magnetic Resonance Research Centre, Centre for Physical Methods of Surface Investigation, Centre for Chemical Analysis and Materials Research, Thermogravimetric and Calorimetric Research Centre.

Appendix A. Supplementary material

Supplementary data to this article can be found online at https://doi.org/10.1016/j.molliq.2022.119043.

References

[1] O.V. Mikolaichuk, V.V. Sharoyko, E.A. Popova, A.V. Protas, A.V. Fonin, L.V. Vasina, Y.A. Anufrikov, M.D. Luttsev, I.A. Nashchekina, A.M. Malkova, G.V. Tochilnikov, S.V. Ageev, K.N. Semenov, Biocompatibility and bioactivity study of a cytostatic drug belonging to the group of alkylating agents of the triazine derivative class, J. Mol. Liq. 343 (2021), https://doi.org/10.1016/j.molliq.2021.117630 117630.

[2] V.B. Duong, P.V. Hien, T.T. Ngoc, P.D. Chau, T.K. Vu, A Simple synthesis of the anticancer drug Altretamine, Lett. Org. Chem. 17 (8) (2020) 628–630, https://doi.org/10.2174/1570178617666200210111041.

[3] C. McIlwain, Triethylenemelamine, in: S.J. Enna, D.B.B.T.T.C.P.R. Bylund (Eds.), XPharm Compr. Pharmacol. Ref., Elsevier, New York, 2008, pp. 1–4. https://doi.org/10.1016/B978-008055232-3.63946-7.

[4] S.K. Vujjini, G. Varanasi, S. Arevelli, S.C. Kandala, S.R. Tirumalaraju, R. Bandichhor, M. Kagga, P. Cherukupally, An Improved and scalable process for the synthesis of 5-Azacytidine: an antineoplastic drug, Org. Process Res. Dev. 17 (2) (2013) 303–306, https://doi.org/10.1021/op300192e.

[5] J. Dubois, R. Arnould, F. Abikhalil, M. Hanocq, G. Atassi, G. Ghanem, A. Libert, F. J. Lejeune, *In vitro* cytotoxicity of hexamethylmelamine (HMM) and its derivatives, Anticancer Res. 10 (1990) 827–832. http://www.ncbi.nlm.nih.gov/pubmed/2114821.

[6] GordonD. Jack, L. Doyle, M.M. Palejwalla, Tretamine in the treatment of inoperable lung cancer, Lancet 275 (7117) (1960) 206–207, https://doi.org/10.1016/S0140-6736(60)90118-5.

[7] T. Kiziltepe, T. Hideshima, L. Catley, N. Raje, H. Yasui, N. Shiraishi, Y. Okawa, H. Ikeda, S. Vallet, S. Pozzi, K. Ishitsuka, E.M. Ocio, D. Chauhan, K.C. Anderson, 5-Azacytidine, a DNA methyltransferase inhibitor, induces ATR-mediated DNA double-strand break responses, apoptosis, and synergistic cytotoxicity with doxorubicin and bortezomib against multiple myeloma cells, Mol. Cancer Ther. 6 (6) (2007) 1718–1727, https://doi.org/10.1158/1535-7163.MCT-07-0010.

[8] P. Singla, V. Luxami, K. Paul, Triazine as a promising scaffold for its versatile biological behavior, Eur. J. Med. Chem. 102 (2015) 39–57, https://doi.org/10.1016/j.ejmech.2015.07.037.

[9] V.G. Bespalov, E.A. Vyshinskaya, I.N. Vasil'eva, A.L. Semenov, M.A. Maidin, N.V. Barakova, A.N. Stukov, Comparative study of antitumor efficiency of intraperitoneal and intravenous cytostatics in experimental rats with disseminated ovarian cancer, Bull. Exp. Biol. Med. 162 (3) (2017) 383–386, https://doi.org/10.1007/s10517-017-3621-5.

[10] A.E. Borisov, M.L. Gershanovich, V.P. Zemlianoĭ, S.L. Nepomniashchaia, A.N. Stukov, V.A. Filov, The use of dioxadet in chemoembolization of the hepatic artery in primary and metastatic cancer of the liver, Vopr. Onkol. 44 (1998) 714–717. http://www.ncbi.nlm.nih.gov/pubmed/10087972.

[11] V.G. Bespalov, A.A. Zhabin, A.N. Stukov, O.A. Beliaeva, Y.G. Murazov, A.L. Semenov, S.A. Kon'kov, I.M. Krylova,, Synergism of antitumor action of dioxadet and cisplatin in model of ascitic ovarian tumor, Sib. J Oncol. 1 (2013) 42–46. https://www.siboncoj.ru/jour/article/view/48/50.

[12] V.A. Filov, A.N. Stukov, L.L. Malyugina, B.A. Ivin, Study of antitumor activity and toxicity of Dioxadet, Experiment. Oncol. 18 (1996) 84–86.

[13] V.G. Bespalov, G.S. Kireeva, O.A. Belyaeva, O.E. Kalinin, K.Y. Senchik, A.N. Stukov, G.I. Gafton, K.D. Guseynov, A.M. Belyaev, Both heat and new chemotherapeutic drug dioxadet in hyperthermic intraperitoneal chemoperfusion improved survival in rat ovarian cancer model, J. Surg. Oncol. 113 (4) (2016) 438–442, https://doi.org/10.1002/jso.24140.

[14] D.K. Latipova, M.L. Gershanovich, A.N. Stukov, T.I. Semiglazova, L.V. Filatova, A. A. Tarasenkova, S.F. Vershinina, S.A. Kon'kov, I.M. Krylova, V.G. Bespalov, A. V Panchenko, I.G. Murazov,, Synergism of antitumor activity of gemcitabine and dioxadet in mice with ascitic Ehrlich's tumor, Vopr. Onkol. 57 (2011) 767–770. http://www.ncbi.nlm.nih.gov/pubmed/22416395.

[15] G. Patrick, An Introduction to Medicinal Chemistry, Oxford University Press, 2017. https://global.oup.com/academic/product/an-introduction-to-medicinal-chemistry-9780198749691?q=An Introduction to Medicinal Chemistry&lang=en&cc=ru.

[16] W. Czechtizky, P. Hamley, Small molecule medicinal chemistry: strategies and technologies, Wiley, 2015. https://www.wiley.com/en-au/Small+Molecule+Medicinal+Chemistry%3A+Strategies+and+Technologies-p-9781118771600.

[17] R.B. Silverman, M.W. Holladay, The Organic Chemistry of Drug Design and Drug Action: Third Edition, Elsevier Inc., 2015. https://doi.org/10.1016/C2009-0-64537-2.

[18] A.V. Kustov, O.A. Antonova, N.L. Smirnova, A.A. Kladiev, A.A. Kladiev, T.V. Kudayarova, M.S. Gruzdev, D.B. Berezin, The energetics of solvation and ion-ion interactions in prospidium chloride aqueous solutions, J. Mol. Liq. 263 (2018) 49–52, https://doi.org/10.1016/j.molliq.2018.04.118.

[19] H. Akbaş, A. Karadağ, A. Aydın, A. Destegül, Z. Kılıç, Synthesis, structural and thermal properties of the hexapyrrolidinocyclotriphosphazenes-based protic molten salts: Antiproliferative effects against HT29, HeLa, and C6 cancer cell lines, J. Mol. Liq. 230 (2017) 482–495, https://doi.org/10.1016/j.molliq.2017.01.067.

[20] T.Y. Nikolaienko, Interaction of anticancer drug doxorubicin with sodium oleate bilayer: Insights from molecular dynamics simulations, J. Mol. Liq. 235 (2017) 31–43, https://doi.org/10.1016/j.molliq.2016.11.065.

[21] A. Jouyban, E. Rahimpour, Z. Karimzadeh, A new correlative model to simulate the solubility of drugs in mono-solvent systems at various temperatures, J. Mol. Liq. 343 (2021) 117587, https://doi.org/10.1016/j.molliq.2021.117587.

[22] J. Gurung, J. Anjudikkal, A.K. Pulikkal, Amphiphilic drug–additive systems in aqueous and organic solvent–water mixed media: A comprehensive account on physicochemical properties, J. Mol. Liq. 318 (2020) 114221, https://doi.org/10.1016/j.molliq.2020.114221.

[23] M. Mondal, S. Basak, S. Choudhury, N.N. Ghosh, M.N. Roy, Investigation of molecular interactions insight into some biologically active amino acids and aqueous solutions of an anti-malarial drug by physicochemical and theoretical approach, J. Mol. Liq. 341 (2021) 116933, https://doi.org/10.1016/j.molliq.2021.116933.

[24] F.A. Alhumaydhi, M.A. Aljasir, A.S.M. Aljohani, S.A. Alsagaby, A.S.S. Alwashmi, M. Shahwan, M.I. Hassan, A. Islam, A. Shamsi, Probing the interaction of memantine, an important Alzheimer's drug, with human serum albumin: *In silico* and *in vitro* approach, J. Mol. Liq. 340 (2021) 116888, https://doi.org/10.1016/j.molliq.2021.116888.

[25] G.M. Sheldrick, SHELXT – Integrated space-group and crystal-structure determination, Acta Crystallogr. Sect. A Found. Adv. 71 (2015) 3–8, https://doi.org/10.1107/S2053273314026370.

[26] G.M. Sheldrick, Crystal structure refinement with SHELXL, Acta Crystallogr. Sect. C Struct. Chem. 71 (2015) 3–8, https://doi.org/10.1107/S2053229614024218.

[27] O.V. Dolomanov, L.J. Bourhis, R.J. Gildea, J.A.K. Howard, H. Puschmann, OLEX2: a complete structure solution, refinement and analysis program, J. Appl. Crystallogr. 42 (2009) 339–341, https://doi.org/10.1107/S0021889808042726.

[28] V.V. Sharoyko, S.V. Ageev, A.A. Meshcheriakov, A.V. Akentiev, B.A. Noskov, I.T. Rakipov, N.A. Charykov, N.A. Kulenova, B.K. Shaimardanova, N.E. Podolsky, K.N. Semenov, Physicochemical study of water-soluble $C_{60}(OH)_{24}$ fullerenol, J. Mol. Liq. 311 (2020) 113360, https://doi.org/10.1016/j.molliq.2020.113360.

[29] E.I. Pochkaeva, A.A. Meshcheriakov, S.V. Ageev, N.E. Podolsky, A.V. Petrov, N.A. Charykov, L.V. Vasina, O.Y. Nikolaeva, I.N. Gaponenko, V.V. Sharoyko, I.V. Murin, K.N. Semenov, Polythermal density and viscosity, nanoparticle size distribution, binding with human serum albumin and radical scavenging activity of the C_{60}-L-arginine ($C_{60}(C_6H_{13}N_4O_2)_8H_8$) aqueous solutions, J. Mol. Liq. 297 (2020) 111915, https://doi.org/10.1016/j.molliq.2019.111915.

[30] S.V. Ageev, G.O. Iurev, N.E. Podolsky, I.T. Rakipov, L.V. Vasina, B.A. Noskov, A.V. Akentiev, N.A. Charykov, I.V. Murin, K.N. Semenov, Density, speed of sound, viscosity, refractive index, surface tension and solubility of $C_{60}[C(COOH)_2]_3$, J. Mol. Liq. 291 (2019), https://doi.org/10.1016/j.molliq.2019.111256 111256.

[31] E.B. Serebryakov, D.N. Zakusilo, K.N. Semenov, N.A. Charykov, A.V. Akentiev, B. A. Noskov, A.V. Petrov, N.E. Podolsky, A.S. Mazur, L.V. Dul'neva, I.V. Murin, Physico-chemical properties of C_{70}-L-threonine bisadduct ($C_{70}(C_4H_9NO_2)_2$)

aqueous solutions, J. Mol. Liq. 279 (2019) 687–699, https://doi.org/10.1016/j.molliq.2019.02.013.
[32] N.E. Podolsky, M.A. Marcos, D. Cabaleiro, K.N. Semenov, L. Lugo, A.V. Petrov, N. A. Charykov, V.V. Sharoyko, T.D. Vlasov, I.V. Murin, Physico-chemical properties of $C_{60}(OH)_{22-24}$ water solutions: Density, viscosity, refraction index, isobaric heat capacity and antioxidant activity, J. Mol. Liq. 278 (2019) 342–355, https://doi.org/10.1016/j.molliq.2018.12.148.
[33] E.B. Serebryakov, K.N. Semenov, I.V. Stepanyuk, N.A. Charykov, A.N. Mescheryakov, A.N. Zhukov, A.V. Chaplygin, I.V. Murin, Physico-chemical properties of the C_{70}-L-lysine aqueous solutions, J. Mol. Liq. 256 (2018) 507–518, https://doi.org/10.1016/j.molliq.2018.02.057.
[34] K.N. Semenov, N.A. Charykov, A.A. Meshcheriakov, E. Lahderanta, A.V. Chaplygin, Y.A. Anufrikov, I.V. Murin, Physico-chemical properties of the C_{60}-L-threonine water solutions, J. Mol. Liq. 242 (2017) 940–950, https://doi.org/10.1016/j.molliq.2017.07.098.
[35] K.N. Semenov, N.A. Charykov, G.O. Iurev, N.M. Ivanova, V.A. Keskinov, D.G. Letenko, V.N. Postnov, V.V. Sharoyko, N.A. Kulenova, I.V. Prikhodko, I.V. Murin, Physico-chemical properties of the C_{60}-L-lysine water solutions, J. Mol. Liq. 225 (2017) 767–777, https://doi.org/10.1016/j.molliq.2016.11.003.
[36] O.S. Manyakina, K.N. Semenov, N.A. Charykov, N.M. Ivanova, V.A. Keskinov, V. V. Sharoyko, D.G. Letenko, V.A. Nikitin, V.V. Klepikov, I.V. Murin, Physico-chemical properties of the water-soluble C_{70}-tris-malonic solutions, J. Mol. Liq. 211 (2015) 487–493, https://doi.org/10.1016/j.molliq.2015.06.071.
[37] A.A. Shestopalova, K.N. Semenov, N.A. Charykov, V.N. Postnov, N.M. Ivanova, V. V. Sharoyko, V.A. Keskinov, D.G. Letenko, V.A. Nikitin, V.V. Klepikov, I.V. Murin, Physico-chemical properties of the C_{60}-arginine water solutions, J. Mol. Liq. 211 (2015) 301–307, https://doi.org/10.1016/j.molliq.2015.07.022.
[38] K.N. Semenov, N.A. Charykov, I.V. Murin, Y.V. Pukharenko, Physico-chemical properties of the C_{60}-tris-malonic derivative water solutions, J. Mol. Liq. 201 (2015) 50–58, https://doi.org/10.1016/j.molliq.2014.11.019.
[39] K.N. Semenov, N.A. Charykov, I.V. Murin, Y.V. Pukharenko, Physico-chemical properties of the fullerenol-70 water solutions, J. Mol. Liq. 202 (2015) 1–8, https://doi.org/10.1016/j.molliq.2014.12.002.
[40] V.V. Sharoyko, S.V. Ageev, A.A. Meshcheriakov, N.E. Podolsky, J.P. Vallejo, L. Lugo, I.T. Rakipov, A.V. Petrov, A.V. Ivanova, N.A. Charykov, K.N. Semenov, Physicochemical investigation of water-soluble $C_{60}(C_2NH_4O_2)_4H_4$ (C_{60}-Gly) adduct, J. Mol. Liq. 344 (2021) 117658, https://doi.org/10.1016/j.molliq.2021.117658.
[41] A.O.E. Abdelhalim, V.V. Sharoyko, A.A. Meshcheriakov, S.D. Martynova, S.V. Ageev, G.O. Iurev, H. Al Mulla, A.V. Petrov, I.L. Solovtsova, L.V. Vasina, I.V. Murin, K.N. Semenov, Reduction and functionalization of graphene oxide with L-cysteine: Synthesis, characterization and biocompatibility, Nanomedicine Nanotechnology, Biol. Med. 29 (2020) 102284, https://doi.org/10.1016/j.nano.2020.102284.
[42] M.J. Blandamer, M.I. Davis, G. Douhéret, J.C.R. Reis, Apparent molar isentropic compressions and expansions of solutions, Chem. Soc. Rev. 30 (2001) 8–15, https://doi.org/10.1039/a908547e.
[43] S. Ebrahimi, R. Sadeghi, Density, speed of sound, and viscosity of some binary and ternary aqueous polymer solutions at different temperatures, J. Chem. Eng. Data. 60 (11) (2015) 3132–3147, https://doi.org/10.1021/acs.jced.5b00290.
[44] L. Šimurka, I. Cibulka, L. Hnědkovský, Partial molar isentropic compressions and partial molar volumes of selected branched aliphatic alcohols at infinite dilution in water at temperatures from T = (278 to 318) K and atmospheric pressure, J. Chem. Eng. Data 57 (5) (2012) 1570–1580, https://doi.org/10.1021/je300175w.
[45] M.S. Alam, B. Ashokkumar, A. Mohammed Siddiq, The density, dynamic viscosity and kinematic viscosity of protic polar solvents (pure and mixed systems) studies: A theoretical insight of thermophysical properties, J. Mol. Liq. 251 (2018) 458–469, https://doi.org/10.1016/j.molliq.2017.12.089.
[46] L.S. Garca-Coln, L.F. del Castillo, P. Goldstein, Theoretical basis for the Vogel-Fulcher-Tammann equation, Phys. Rev. B 40 (10) (1989) 7040–7044, https://doi.org/10.1103/PhysRevB.40.7040.
[47] B.V. Ioffe, Refractometry as a method for the physicochemical analysis of organic systems, Russ. Chem. Rev. 29 (2) (1960) 53–66.
[48] I. Apok, M. Bartok, R.A. Karakhanov, N.I. Shuikin, Chemical properties of 1,3-dioxans, Russ. Chem. Rev. 38 (1) (1969) 37–46, https://doi.org/10.1070/RC1969v038n01ABEH001723.
[49] Dioxadet | $C_{14}H_{22}N_6O_3$ – PubChem, (n.d.). https://pubchem.ncbi.nlm.nih.gov/compound/48858.
[50] T. Cheng, Y. Zhao, X. Li, F. Lin, Y. Xu, X. Zhang, Y. Li, R. Wang, L. Lai, Computation of octanol–water partition coefficients by guiding an additive model with knowledge, J. Chem. Inf. Model. 47 (6) (2007) 2140–2148.
[51] Y. Pommier, E. Leo, HongLiang Zhang, C. Marchand, DNA Topoisomerases and Their Poisoning by Anticancer and Antibacterial Drugs, Chem. Biol. 17 (5) (2010) 421–433, https://doi.org/10.1016/j.chembiol.2010.04.012.
[52] O. Akiyode, D. George, G. Getti, J. Boateng, Systematic comparison of the functional physico-chemical characteristics and biocidal activity of microbial derived biosurfactants on blood-derived and breast cancer cells, J. Colloid Interface Sci. 479 (2016) 221–233, https://doi.org/10.1016/j.jcis.2016.06.051.
[53] A. Amuthan, V. Devi, C.S. Shreedhara, V. Rao, R. Lobo, Cytoprotective Activity of Neichitti (Vernonia cinerea) in Human Embryonic Kidney (HEK293) Normal Cells and Human Cervix Epitheloid Carcinoma (HeLa) Cells against Cisplatin Induced Toxicity: A Comparative Study, J. Clin. Diagnostic Res. 13 (2019) KC01–KC06. https://doi.org/10.7860/JCDR/2019/40242.12624.
[54] Z. Farhane, F. Bonnier, O. Howe, A. Casey, H.J. Byrne, Doxorubicin kinetics and effects on lung cancer cell lines using *in vitro* Raman micro-spectroscopy: binding signatures, drug resistance and DNA repair, J. Biophotonics 11 (1) (2018) e201700060, https://doi.org/10.1002/jbio.201700060.
[55] Drug: Cisplatin – Cancerrxgene – Genomics of Drug Sensitivity in Cancer, (n.d.). https://www.cancerrxgene.org/compound/Cisplatin/1005/by-tissue?
[56] Drug: Doxorubicin – Cancerrxgene – Genomics of Drug Sensitivity in Cancer, (n.d.). https://www.cancerrxgene.org/compound/Doxorubicin/133/by-tissue?
[57] K. Gorshkov, N.i. Sima, W. Sun, B. Lu, W. Huang, J. Travers, C. Klumpp-Thomas, S.G. Michael, T. Xu, R. Huang, E.M. Lee, X. Cheng, W. Zheng, Quantitative chemotherapeutic profiling of gynecologic cancer cell lines using approved drugs and bioactive compounds, Transl. Oncol. 12 (3) (2019) 441–452, https://doi.org/10.1016/j.tranon.2018.11.016.
[58] S. Zheng, X. Wang, Y.-H. Weng, X. Jin, J.-L. Ji, L. Guo, B. Hu, N. Liu, Q. Cheng, J. Zhang, H. Bai, T. Yang, X.-H. Xia, H.-Y. Zhang, S. Gao, Y. Huang, siRNA Knockdown of RRM2 effectively suppressed pancreatic tumor growth alone or synergistically with doxorubicin, Mol. Ther. – Nucleic Acids. 12 (2018) 805–816, https://doi.org/10.1016/j.omtn.2018.08.003.
[59] M. Beer, N. Kuppalu, M. Stefanini, H. Becker, I. Schulz, S. Manoli, J. Schuette, C. Schmees, A. Casazza, M. Stelzle, A. Arcangeli, A novel microfluidic 3D platform for culturing pancreatic ductal adenocarcinoma cells: comparison with in vitro cultures and *in vivo* xenografts, Sci. Rep. 7 (2017) 1–12, https://doi.org/10.1038/s41598-017-01256-8.
[60] J.-C. Hahm, I.-K. Lee, W.-K. Kang, S.-U. Kim, Y.-J. Ahn, Cytotoxicity of neolignans identified in Saururus chinensis towards human cancer cell lines, Planta Med. 71 (5) (2005) 464–469.